J. Cell. Mol. Med. Vol 13, No 8B, 2009 pp. 2602-2612

Simple application of fibronectin–mimetic coating enhances osseointegration of titanium implants

Timothy A. Petrie, Catherine D. Reyes, Kellie L. Burns, Andrés J. García *

Woodruff School of Mechanical Engineering and Petit Institute for Bioengineering and Bioscience, Georgia Institute of Technology, Atlanta, GA, USA

Received: May 9, 2008; Accepted: August 12, 2008

Abstract

Integrin-mediated cell adhesion to biomolecules adsorbed onto biomedical devices regulates device integration and performance. Because of the central role of integrin-fibronectin (FN) interactions in osteoblastic function and bone formation, we evaluated the ability of FN-inspired biomolecular coatings to promote osteoblastic differentiation and implant osseointegration. Notably, these biomolecular coatings relied on physical adsorption of FN-based ligands onto biomedical-grade titanium as a simple, clinically translatable strategy to functionalize medical implants. Surfaces coated with a recombinant fragment of FN spanning the central cell binding domain enhanced osteoblastic differentiation and mineralization in bone marrow stromal cell cultures and increased implant osseointegration in a rat cortical bone model compared to passively adsorbed arginine–glycine–aspartic acid peptides, serum proteins and full-length FN. Differences in biological responses correlated with integrin binding specificity and signalling among surface coatings. This work validates a simple, clinically translatable, surface biofunctionalization strategy to enhance biomedical device integration.

Keywords: fibronectin • osseointegration • coating • integrins • biomimetic • implant

Introduction

Current orthopaedic implant surface technologies, including porous coatings and calcium phosphate overcoats, seek to promote bone cell ingrowth and mineral formation [1–3]. Although these approaches are successful in many cases, they can be restricted by slow rates of osseointegration and poor mechanical anchorage, especially in challenging clinical cases, such as those associated with large bone loss and poor bone quality [4]. In addition, these surface modification approaches rely on costly and manufacturing-intensive processes. As an alternative to these surface technologies, emerging biomimetic strategies have focused on the presentation of biological motifs, including extracellular matrix (ECM) sequences and growth factors [5–16]. The general paradigm of these bio-inspired approaches is the covalent immobilization (tethering) of the biological entities onto the underlying material support, which often involves multistep procedures to render the support suitable for biofunctionalization [17, 18]. In contrast, we recently described a simple, one-step coating procedure that relies on the passive adsorption of a synthetic collagen-based peptide onto biomedical grade titanium (Ti) to enhance osseointegration [19].

Integrins are a large family of heterodimeric ($\alpha\beta$) transmembrane receptors that mediate cell-matrix and cell–cell adhesion and trigger signals regulating cell survival, proliferation and differentiation [20–24]. Osteoprogenitor cells and osteoblasts express a wide panel of integrins, including $\alpha_5\beta_1$, $\alpha_v\beta_3$, $\alpha_3\beta_1$, $\alpha_8\beta_1$ and $\alpha_2\beta_1$, which mediate interactions with collagens [25, 26], fibronectin (FN) [27, 28], laminins [29] and other matrix components [30, 31]. Specific integrin-ECM adhesive interactions regulate osteoblast function and mineralization [32–36]. Importantly, osteoblast integrin-ECM interactions are dynamic, and the extent of early and late mineralization is dependent on the particular integrin-matrix protein interactions engaged [27, 37–39].

Because of the central roles of integrin-ECM interactions in osteoblast activities, integrins represent an attractive target in the design of biofunctionalized orthopaedic implants [18]. The large majority of these efforts have centred on presenting short binding motifs incorporating the arginine–glycine–aspartic acid (RGD) minimal binding sequence from FN, bone sialoprotein and osteopontin [40–42]. Despite improved adhesion and differentiation *in vitro*,

*Correspondence to: Andrés J. GARCÍA,
Woodruff School of Mechanical Engineering, 315 Ferst Drive,
Room 2314 IBB, Atlanta, GA 30332-0363, USA.
Tel.: 404–894-9384
Fax: 404–385-1397
E-mail: andres.garcia@me.gatech.edu

doi:10.1111/j.1582-4934.2008.00476.x

implant surfaces presenting RGD motifs do not consistently enhance osseointegration and bone formation in animal models [40, 43–45]. In the present work, we evaluated the ability of different FN-inspired biomolecular coatings to promote *in vitro* osteoblastic differentiation and implant osseointegration in a rat cortical bone model. Notably, these biomolecular coatings rely on simple physisorption of FN-based ligands onto biomedical-grade Ti as a simple, clinically translatable, implant biofunctionalization strategy.

Methods

Bioadhesive ligands and preparation of surfaces

The bioadhesive ligands examined in this study were: (*i*) a recombinant fragment spanning the 7th–10th type III repeats of human fibronectin ($FNIII_{7–10}$), (*ii*) human plasma fibronectin (pFN) and (*iii*) a linear RGD peptide (GRGDSPC). $FNIII_{7–10}$ was expressed in *E. coli* and purified as previously described [46]. Briefly, JM109 cells were transformed with plasmid encoding for biotinylated $FNIII_{7–10}$, streaked onto agar plates, colonies isolated and cultures grown overnight in standard lysogeny broth (LB) Broth. Cells were lysed *via* lysozyme/sonication and the $FNIII_{7–10}$ was purified by affinity chromatography on a monomeric avidin column by elution with d-biotin (Pierce, Rockford, IL, USA). Purity was >95% as assessed by SDS-PAGE and Ponceau solution staining. After further filtering with 30 kD Microcon centrifugal filter devices (Millipore, Bedford, MA, USA) to remove excess d-biotin, purity was determined to be >98%. $FNIII_{7–10}$ was maintained in a stock solution of Dulbecco's phosphate buffered saline at 2 mg/ml (PBS; Invitrogen, Carlsbad, CA, USA). Human pFN was purchased from Invitrogen (catalogue #33016) and reconstituted in aliquots of sterile distilled water. Purity was assessed by SDS-PAGE by Invitrogen Quality Control at >95%. The RGD peptide was obtained from BACHEM (Torrance, CA, USA, catalogue #H-7245), reconstituted in 0.1% trifluoroacetic acid and assessed as >98% pure.

Titanium metal was obtained from Kurt J. Lesker Company Part #EVMTI137EXE (Clairton, PA, USA) as pellets of 99.97% pure Ti. For *in vitro* assays, thin films (300 Å) of this Ti were deposited onto clean glass cover slips using an electron bean evaporator (2×10^{-6} Torr) at a deposition rate of 1 Å/sec. Slides were then immersed in a $FNIII_{7–10}$, pFN, or RGD peptide solution at various coating concentrations in PBS for 30 min. Surfaces were subsequently blocked with 1% heat denatured bovine serum albumin (BSA). For the *in vivo* experiments, implants were machined from commercially pure, clinical-grade (grade 4) Ti rods (Titanium Industries, Inc., Cleveland OH, USA). Ligand surface density measurements were obtained *via* surface plasmon resonance (SPR) using a Biacore X instrument. For subsequent cell-based experiments, $FNIII_{7–10}$ and pFN were coated on Ti surfaces at equimolar (RGD binding site) surface densities as determined by SPR. Other surfaces were either exposed to serum or RGD peptide (50 μg/ml) for 30 min.

Cell adhesion, integrin binding and signalling assays

Primary rat bone marrow stromal cells (rBMSCs), a heterogeneous cell population containing osteoprogenitors and which represents an analogous cell source to human bone marrow stromal cells currently used in clinical applications [47, 48], were selected as the cell model to examine this biomimetic coating technology. rBMSCs were isolated and cultured under IACUC-approved procedures [20]. Cells were passaged no more than three times after rat isolation in growth medium (α-minimum essential medium (MEM) + 10% foetal bovine serum + 1% penicillin-streptomycin) before usage in all *in vitro* experiments. During culture, cells were split prior to 90% confluence, typically every 3 days. Cell adhesion to ligand-adsorbed Ti surfaces under serum-free conditions was measured at 1 hr adhesion time at 37°C using a centrifugation assay [49]. For integrin blocking experiments, cells were incubated in the presence of 20 μg/ml anti-rat α_5 integrin (CD49e, clone HMα5–1, BD Biosciences, San Diego, CA, USA) or anti-rat α_V (CD51, clone 21, BD Biosciences, San Diego, CA, USA) blocking antibodies for 20 min. prior to cell seeding, and seeded for 1 hr adhesion time.

Integrin binding levels (after 30 min. adhesion) were assessed using a crosslinking/extraction/reversal procedure [50]. This procedure uses 3,3′-Dithiobis[sulfosuccinimidylpropionate] (DTSSP) to specifically crosslink integrins bound to their ligand. Cellular components are then extracted using detergent and protease inhibitors, and crosslinks are reversed and the once-bound integrins are collected. Integrin levels were quantified by Western blotting using primary antibodies against α_5 integrin (AB1928, Chemicon, Chemicon, Bedford, MA, USA; 0.5 μg/ml), and α_V integrin (AB1930, Chemicon, Chemicon, Bedford, MA, USA; 0.5 μg/ml). Membranes were washed in TBS-Tween (20 mM Tris HCl pH 7.6, 137 mM NaCl, 0.1% Tween 20) for 45 min. and incubated in secondary antibody (biotin-conjugated anti-rabbit IgG, 1:20,000 dilution in Blotto) for 1 hr at room temperature while rocking. Membranes were washed again in tri-buffered saline (50 mM Tris, pH 7.6) (TBS)-Tween for 45 min. and incubated in a tertiary antibody (alkaline phosphatase-conjugated anti-biotin immunoglobulin G antibody (IgG), 1:10,000 dilution in Blotto) for 1 hr at room temperature while rocking. After antibody incubation, membranes were washed in TBS-Tween for 45 min. and immunoreactivity was detected using an ECF™ fluorescent substrate for 5–10 min. Bands were visualized using a Fuji Image Analyzer (FujiFilm FLA-3000 Image Analyzer, FujiFilm, USA, Norcross, GA, USA) and further quantified and analysed using Adobe Photoshop software.

For focal adhesion kinase (FAK) activation experiments, rBMSCs were incubated in serum-free suspension (αMEM + 5% BSA) for 30 min. to reduce FAK background activation and then in the presence or absence of integrin blocking antibodies for 20 min. prior to cell seeding for 2 hrs at 37°C. Cells were lysed in cold radio immuno precipitation assay (RIPA) buffer (1% Triton X-100, 1% sodium deoxycholate, 0.1% SDS, 150 mM NaCl, 150 mM Tris-HCl [pH 7.2], 350 μg/ml phenylmethanesulphonyl fluoride (PMSF), 10 μg/ml leupeptin, 10 μg/ml aprotonin) on ice for 15 min. FAK activation was subsequently quantified *via* Western blotting using primary antibodies against specific phosphorylated FAK tyrosine residues (pY397, pY576, pY861 in Blotto for 1 hr) and total FAK (anti-FAK). Bands were visualized and quantified in the same manner as the integrin binding procedure. FAK phosphorylation levels were normalized to the amount of total FAK for each experimental condition.

Proliferation assay

After plating for 16 hrs in 10% serum, cells were incubated in bromodeoxyuridine (BrdU) (3.1 μg/ml) for 4 hrs. Samples were fixed in 70% ethanol, denatured in 4 M HCl, neutralized in 100 mM Tris-HCl + 50 mM NaCl and blocked with 5% foetal bovine serum. Samples were then incubated with anti-BrdU (1:1000) and AF488 anti-mouse IgG (1:200) as well as Hoechst dye (1:10,000) to stain nuclei. Using in-house image analysis, the number of cells positive for BrdU relative to total cell nuclei was quantified.

Osteoblast-specific gene expression

rBMSCs at low passage were seeded on appropriate surfaces at 200 cells/mm^2 in growth medium (α-MEM + 10% foetal bovine serum + 1% penicillin-streptomycin). After 24 hrs, cultures were switched to osteogenic medium consisting of growth medium supplemented with 50 μg/ml L-absorbic acid and 3 mM sodium β-glycerophosphate. Total RNA was isolated at day 7 using Qiagen RNEasy kits (Qiagen, Valencia, CA, USA). cDNA synthesis was performed on DNAase I-treated (25 Kunitz units) RNA by oligo(dT) priming *via* SuperScript II pre-amplification system (Invitrogen). Real-time PCR was performed with an Applied Biosystems ABI Prism 7700 (Applied Biosystems, Foster City, CA, USA) using osteoblast-specific primers and SYBR© green intercalating dye [20]. Transcript concentration was quantified from a linear curve of standards, which were amplified from cDNA *via* oligonucleotide primers for each gene assayed (Runx2, bone sialoprotein [BSP] and osteocalcin [OCN]).

Alkaline phosphate (ALP) activity and matrix mineralization assays

ALP activity was quantified biochemically at 7 days after seeding. Protein was isolated from cell cultures and equal amounts (2.5 μg) were added to 5-methyl umbelliferyl phosphate fluorescent substrate (60 μg/ml) for 60 min. Fluorescence was measured (360 nm/465 nm) and enzymatic activity normalized to total amount of protein. Calcium content was analysed at 7 days in culture by dissolving mineralized deposits overnight in 1.0 N acetic acid and using a calcium-detecting reagent (Diagnostic Chemicals Ltd., Charlottetown, Prince Edward Island, Canada). Mineralization analyses were conducted by von Kossa staining 14-day cultures, and percentage mineralization was quantified by image analysis.

Implantation procedure and functional analysis

Implantations into the tibiae of mature Sprague-Dawley male rats were conducted in accordance with an IACUC-approved protocol as described previously [19]. A day before implantation, Ti implants were soaked in de-ionized water for 30 min., and subsequently stripped of the existing oxide layer by submersion in 4% hydrofluoric acid (HF) for 30 sec. A new oxide layer was formed by incubation of implants in 35% HNO_3. This cleaning and re-growth of the oxide layer can be performed days before implantation as long as samples are subsequently kept clean. This stripping and re-growth of the Ti oxide layer was done to generate clean and well-defined surfaces and have surfaces equivalent to what is used in clinical implants. This cleaning step is not required for adsorption of bioactive peptides. At the time of surgery, implants were coated with ligand by incubating in ligand solutions in PBS for 30 min. Tapered Ti implants treated with FNIII$_{7–10}$ or pFN at equimolar RGD-coating density (0.8 pmol/cm^2) or unmodified Ti were press fit into the cortical defects. Two 2-mm-diameter defects were drilled into the medial aspect of the proximal tibial metaphysis of each leg to achieve a total of four implants per animal (Fig. 6A and B). Implant locations (R/L leg, proximal/distal location) were randomized for each surface condition (pFN, FNIII$_{7–10}$, unmodified Ti) and a total of 11 rats were used. After 4 weeks of implantation [19], the rat tibiae were harvested and assessed for bone apposition and implant mechanical fixation. Proximal tibiae were explanted and either fixed in neutral buffered formalin for histology or wrapped in PBS to maintain moisture for immediate mechanical testing. Formalin-fixed tibiae were embedded in poly(methyl methacrylate), dehydrated and stained with Sanderson's Rapid Bone Stain^{TM} and a van Gieson counterstain. Bone apposition was quantified as the percentage of the implant's surface in contact with the bone, and eight fields per implant were quantified ($N = 4$ implants per condition). Pull-out testing was performed to quantify implant mechanical fixation to surrounding bone tissue using an EnduraTEC Bose ELF 3200 (Bose Corporation, Eden Prairie, MN, USA). The ends of each excised tibia were secured using a customized holding apparatus and the exposed head of the implant attached to a load cell *via* a customized grip apparatus. Pre-loaded samples ($<$2 N) were then subjected to a constant pull rate of 0.2 N/sec. The pull-out force (N), parallel to the long axis of implant, was the maximum load achieved before implant detachment or failure.

Statistics

Results are presented as mean $\pm$ standard error. Quantification of *in vitro* and *in vivo* experiments was performed on all samples used in each experiment. Results were analysed by ANOVA in SYSTAT 8.0 (SPSS). If deemed significant, pairwise comparisons were performed using Tukey's post hoc test and a confidence level of 95% was considered significant. *In vitro* assays were conducted in at least triplicate and replicated in two separate experiments.

Results

FN-mimetic ligand implant coatings

Ti surfaces were either exposed to serum or passively coated with one of three biomimetic ligands: (1) FNIII$_{7–10}$, a recombinant fragment of FN spanning the central cell binding domain that promotes $\alpha_5\beta_1$-mediated cell adhesion and signalling [47]. This domain contains the central integrin binding domain comprising the RGD and PHSRN synergy motifs that are essential for high affinity $\alpha_5\beta_1$ binding. (2) Full-length pFN, which is a dimer comprising multiple cell receptor binding sites. (3) A linear RGD-containing peptide. Importantly, the FNIII$_{7–10}$ fragment reconstitutes the 3-D presentation of both the RGD and PHSRN sequences found in pFN, excluding most of the additional adhesion and binding domains also present in pFN [51]. Adsorbed densities were measured by SPR. As expected, adsorbed ligand density increased with ligand-coating concentration exhibiting linear increases at low coating concentrations and reaching saturation values at high coating concentrations, described accurately by hyperbolic curve fits (Fig. 1A). For all subsequent experiments, ligand-coating concentrations were adjusted to yield equimolar surface densities (0.8 pmol/cm^2) of adhesive (RGD) sites in order to directly compare FNIII$_{7–10}$ (45 ng/cm^2) to pFN (125 ng/cm^2). The linear RGD peptide was also considered for comparison as a ligand coating but exhibited poor adsorption efficiency. Minimal RGD peptide densities (below the SPR detection limit 0.1 $\pm$ 0.07 ng/cm^2 corresponding to 0.08 pmol/cm^2) were measured (50 μg/ml coating concentration). The density of adsorbed biomolecules for serum-exposed surfaces was 195 ng/cm^2.

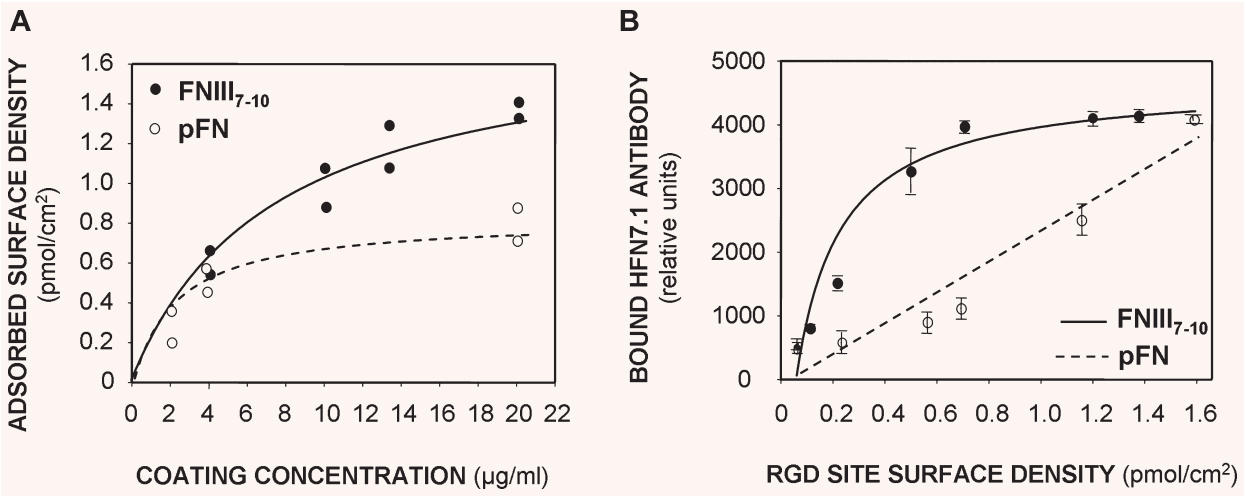

Fig. 1 Surface density and accessibility of bioactive integrin ligands adsorbed on titanium surfaces. (**A**) Adsorbed surface densities of pFN and $FNIII_{7–10}$ to Ti surfaces as measured by surface plasmon resonance. A total of at least eight independent measurements for each peptide were performed. The tethering profile was fit to a simple hyperbolic curve ($FNIII_{7–10}$ curve $R^2 = 0.94$; pFN curve: $R^2 = 0.96$). (**B**) ELISA using $\alpha_5\beta_1$-mimetic HFN 7.1 antibody demonstrating accessibility differences on $FNIII_{7–10}$ and pFN-adsorbed Ti surfaces (hyperbolic curve fit, $FNIII_{7–10}$ curve: $R^2 = 0.97$; pFN curve: $R^2 = 0.95$).

An ELISA using the HFN 7.1 antibody, a mimetic of $\alpha_5\beta_1$ binding to FN [52], verified that both $FNIII_{7–10}$ and pFN adsorbed in a bioactive orientation which is highly accessible to integrin binding (Fig. 1B). Moreover, the antibody-binding curve for adsorbed $FNIII_{7–10}$ on Ti was shifted upwards and to the left compared to the pFN curve, indicating that the average $FNIII_{7–10}$ orientation is more accessible to $\alpha_5\beta_1$ binding than adsorbed pFN. We did not perform ELISA measurements for serum-treated Ti because various RGD-containing proteins adsorb onto Ti from serum [53].

FN-mimetic ligand surfaces promote integrin-specific cell adhesion and signalling

To probe for the main integrin receptors actively engaged during adhesion, a centrifugation cell adhesion assay was performed in the presence and absence of integrin-specific blocking antibodies. rBMSCs displayed greater levels of adhesion to $FNIII_{7–10}$-coated surfaces compared to Ti surfaces exposed to RGD or serum-treated Ti ($P < 0.008$), and adhesion levels were equivalent to pFN-adsorbed surfaces (Fig. 2A). Because the *in vitro* adhesion assay is performed under serum-free conditions, the serum-exposed Ti surface was included to correspond to the untreated Ti surfaces in subsequent *in vitro* assays performed in the presence of serum. Control experiments demonstrated no differences in adhesion between cells plated under serum-free conditions on surfaces pre-exposed to 10% serum and cells seeded on untreated Ti in the presence of serum. Hence, the untreated (in the presence of serum) and serum-exposed surfaces are equivalent in terms of cell adhesion. Cell adhesion on RGD-exposed surfaces was not different from background levels, corroborating the SPR results that this short peptide cannot stably adsorb to Ti. Importantly, a blocking anti-α_5 antibody effectively eliminated cell adhesion to $FNIII_{7–10}$ surfaces ($P < 0.008$), verifying the specificity of this surface for $\alpha_5\beta_1$ integrin, but did not significantly reduce adhesion to pFN-coated or serum-treated surfaces. Conversely, a blocking anti-α_v antibody significantly reduced adhesion to the serum-exposed Ti surface ($P < 0.02$), indicating that adhesion to this surface is mediated primarily by α_v-containing integrins. These data also reflect the ability of Ti to adsorb many RGD-containing serum proteins, including vitronectin, which is recognized mainly by the $\alpha_v\beta_3$ integrin.

We next examined integrin binding to further characterize the adhesion mechanism to ligand-coated implant surfaces. Bound levels of α_5 and α_v integrins (after 45 min. adhesion) were quantified using a biochemical crosslinking/extraction/reversal technique. This robust technique utilizes a water-soluble crosslinker that isolates bound integrin-ligand pairs, and allows direct quantification of the total bound number of integrins. Consistent with the integrin blocking antibody experiments, cells displayed higher levels of bound α_5 on $FNIII_{7–10}$ surfaces over pFN ($P < 0.03$) or Ti-serum ($P < 0.005$) surfaces, whereas higher levels of α_v integrin were engaged on pFN ($P < 0.03$) and serum-treated Ti surfaces ($P < 0.001$) compared to $FNIII_{7–10}$-coated Ti (Fig. 2B). Taken together, these data establish that the $FNIII_{7–10}$-adsorbed surfaces mainly support $\alpha_5\beta_1$-mediated adhesion, whereas the serum-treated and pFN surfaces engage α_v-containing integrins, most likely $\alpha_v\beta_3$.

To examine early integrin-mediated signalling on these supports, we analysed phosphorylation levels of important FAK tyrosines. FAK is an intracellular signalling molecule implicated in

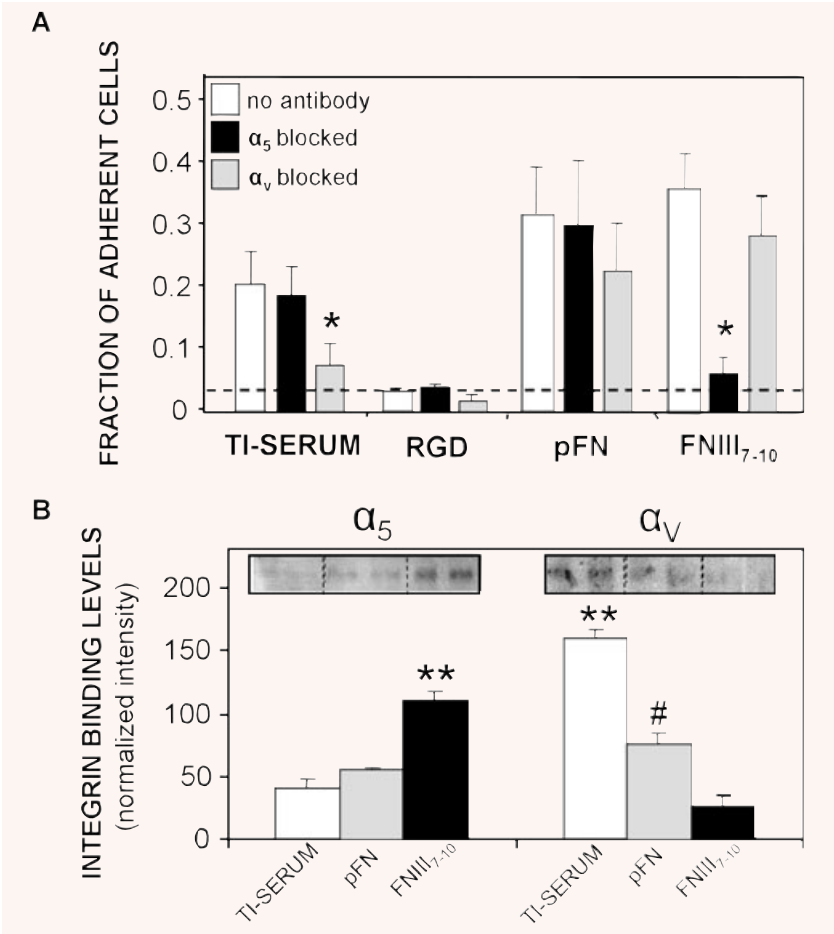

Fig. 2 Titanium (Ti) surfaces functionalized with bioactive integrin ligands display integrin specificity. (**A**) Bone marrow stromal cell adhesion (30 min.) to adsorbed ligand surfaces is mediated by different integrin receptors as demonstrated by blocking antibodies in a cell centrifugation assay. Hashed line represents adhesion levels of cells on Blotto-blocked surfaces and no ligand ($N = 4$). Ti-serum: $^{*}P < 0.02$ *versus* no antibody control; FNIII$_{7–10}$: $^{*}P < 0.008$ *versus* no antibody control. (**B**) Integrin binding analysis using a crosslinking/extraction/reversal procedure for stromal cells plated on ligand-treated Ti surfaces of equimolar density ($N = 5$). α_5: $^{**}P < 0.03$ *versus* pFN, $^{**}P < 0.005$ *versus* Ti-serum; α_V: $^{**}P < 0.01$ *versus* pFN, $^{**}P < 0.001$ *versus* FNIII$_{7–10}$; $^{\#}P < 0.03$ *versus* FNIII$_{7–10}$.

integrin-mediated signal transduction and is directly involved in the osteogenic differentiation pathway [54]. We assessed the phosphorylation of two important residues in FAK: tyrosine 397 (the autophosphorylation site of FAK) and tyrosine 576 (essential for maximal kinase activity) for cells plated on implant surfaces in the presence of integrin blocking antibodies. FAK phosphorylation levels for Y397 and Y576 were enhanced on FNIII$_{7–10}$ surfaces compared to pFN-coated ($P < 0.01$) or Ti-serum surfaces ($P < 0.01$) (Fig. 3A and B). Furthermore, when rBMSCs were pre-incubated with blocking antibodies against β_3, phosphorylation levels of Y397 and Y576 were significantly reduced compared to unblocked controls for cells adhering to either pFN-coated or serum-coated Ti surfaces. Importantly, blocking antibodies against α_5 reduced phosphorylation of FAK tyrosine 397 and 576 residues for cells only on FNIII$_{7–10}$-coated surfaces; blocking α_5 did not produce a significant effect for the other surfaces. These data indicate that the specific integrins engaged during early adhesive events, primarily $\alpha_5\beta_1$ for FNIII$_{7–10}$-coated surfaces and $\alpha_v\beta_3$ for pFN- and serum-coated surfaces, differentially modulate downstream signalling pathways (such as FAK activation) that may be a prerequisite for bone cell differentiation.

Integrin-specific Ti coatings modulate *in vitro* osteogenic activities

We postulated that differences in integrin binding specificity and FAK activation modulate particular cell responses, including proliferation and expression of osteogenic markers. Indeed, a short-term (16 hrs) proliferation assay based on BrdU incorporation demonstrated that cells on FNIII$_{7–10}$-treated Ti surfaces exhibited increased proliferation rates compared to pFN-coated ($P < 0.05$) or serum-treated Ti surfaces ($P < 0.004$) (Fig. 3C). In addition, cells displayed a significantly higher proliferation rate on pFN-coated surfaces over serum-treated Ti ($P < 0.009$). To examine if these integrin-specific adhesive and signalling cues influence osteoblastic differentiation, we used quantitative RT-PCR to monitor osteoblast-specific gene expression in 7-day rBMSC cultures. Expression levels of Runx2/Cbfa1, a transcription factor involved in early osteoblastic differentiation [55], were significantly elevated on FNIII$_{7–10}$-treated surfaces compared to pFN ($P < 0.006$) or serum-treated Ti ($P < 0.03$) (Fig. 4A). Moreover, RT-PCR for late differentiation markers of osteoblastic differentiation, namely OCN and BSP, revealed greater levels of gene expression on FNIII$_{7–10}$

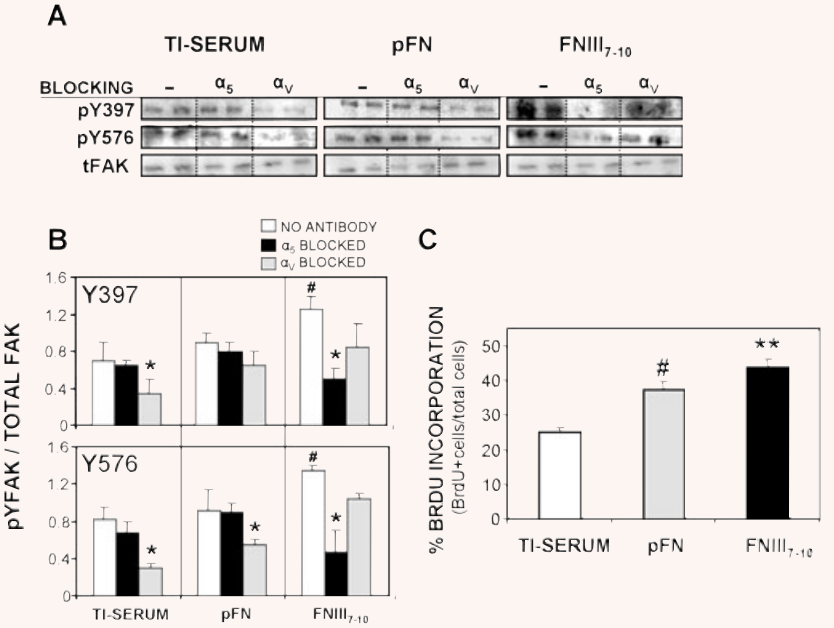

Fig. 3 Initial cell signaling (focal adhesion kinase [FAK] activation) and proliferation on equimolar ligand-treated and serum-treated Ti surfaces is integrin-dependent. (**A**) Relative levels of phospho-Y in FAK were quantified, in the presence or absence of integrin blocking antibodies prior to cell seeding (2 hrs), by Western blotting of cell lysates. Representative blots of each surface condition are shown ($N = 4$). (**B**) Activation levels for Y397 and Y576 (normalized to total FAK) were higher on $FNIII_{7–10}$-coated surfaces than pFN-treated and Ti-serum supports after 2 hrs cell adhesion (Y397: $^{\#}P < 0.01$; Y576: $^{\#}P < 0.01$). Integrin blocking antibodies selectively reduced FAK phosphorylation. Y397: $^{*}P < 0.05$ *versus* no antibody control (Ti-serum), $^{*}P < 0.01$ *versus* no antibody control ($FNIII_{7–10}$); Y576: $^{*}P < 0.02$ *versus* no antibody control (Ti-serum), $^{*}P < 0.05$ *versus* no antibody control (pFN), $^{*}P < 0.03$ *versus* no antibody control ($FNIII_{7–10}$). (**C**) $FNIII_{7–10}$-treated surfaces display higher proliferation rate (%BrdU + cells/total cells) than pFN-coated or Ti-serum surfaces (16 hrs adhesion) ($FNIII_{7–10}$: $^{**}P < 0.05$ *versus* pFN, $^{**}P < 0.004$ *versus* Ti-serum). pFN-treated surfaces also enhanced proliferation rate over serum-treated Ti ($^{\#}P < 0.009$) ($N = 5$).

surfaces compared with serum-treated or pFN-coated Ti surfaces (Fig. 4B). Notably, transcript levels were not statistically different between pFN- and serum-treated Ti surfaces for any of the three genes examined.

We next examined ALP activity and calcium deposition as markers of osteoblastic differentiation. Cells on $FNIII_{7–10}$-surfaces displayed a roughly twofold increase in levels of both ALP activity and calcium-based mineral deposition compared to pFN-coated or serum-treated Ti (Fig. 5A and B). No differences were observed between pFN-treated Ti and serum-exposed Ti for ALP, but levels of calcium mineral levels were significantly higher on pFN surfaces compared to the serum-treated Ti ($P < 0.04$). Moreover, when the mineralized nodules were visualized and quantified after 14 days after cell seeding *via* von Kossa staining, $FNIII_{7–10}$ surfaces supported the highest levels of nodule formation ($P < 0.04$ *versus* pFN; $P < 0.005$ *versus* Ti-serum), followed by pFN surfaces ($P < 0.03$ *versus* Ti-serum), and finally serum-treated Ti surfaces (Fig. 5C). In addition, RGD peptide-incubated Ti surfaces displayed no significant differences in calcium incorporation or von Kossa staining (data not shown) from serum-treated Ti surfaces; we attribute these results to the inadequate adsorption behaviour of the RGD peptide on Ti. Taken together, these results indicate that various biomolecular coatings of different integrin specificity elicit distinct osteoblastic responses *in vitro.*

Integrin $\alpha_5\beta_1$-specific bioactive coatings enhance implant osseointegration

To evaluate the performance of these integrin-specific coatings *in vivo*, we quantified osseointegration of implants in a rat tibial cortical bone model using quantitative histomorphometry and pull-out mechanical testing (Fig. 6A and B) [19]. Extensive, adjoining bone matrix was visible in histological sections around $FNIII_{7–10}$-treated Ti implants, whereas less substantial and more scattered areas of mineral were present around the pFN treated and, especially, the uncoated Ti implants (Fig. 6C). Moreover, image quantification (eight fields per implant; $N = 4$ implants per

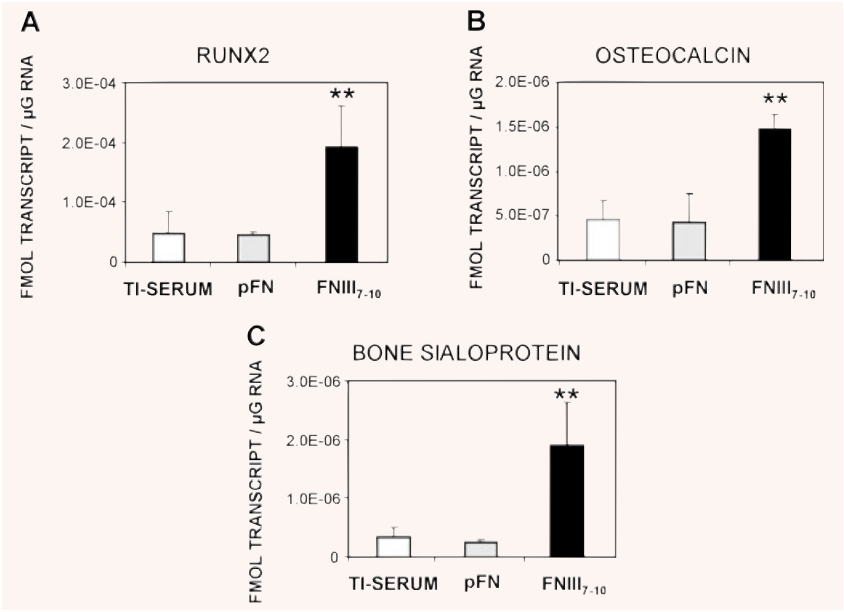

Fig. 4 $FNIII_{7–10}$-treated surfaces enhance expression of osteoblast-specific genes in bone marrow stromal cultures at 7 days after seeding. Gene expression levels for: (**A**) Runx2 transcription factor ($FNIII_{7–10}$: $^{**}P < 0.006$ *versus* pFN, $^{**}P < 0.03$ *versus* Ti-serum), (**B**) osteocalcin ($FNIII_{7–10}$: $^{**}P < 0.02$ *versus* pFN, $^{**}P < 0.01$ *versus* Ti-serum) and (**C**) bone sialoprotein ($FNIII_{7–10}$: $^{**}P < 0.01$ *versus* pFN, $^{**}P < 0.02$ *versus* Ti-serum) ($N = 4$).

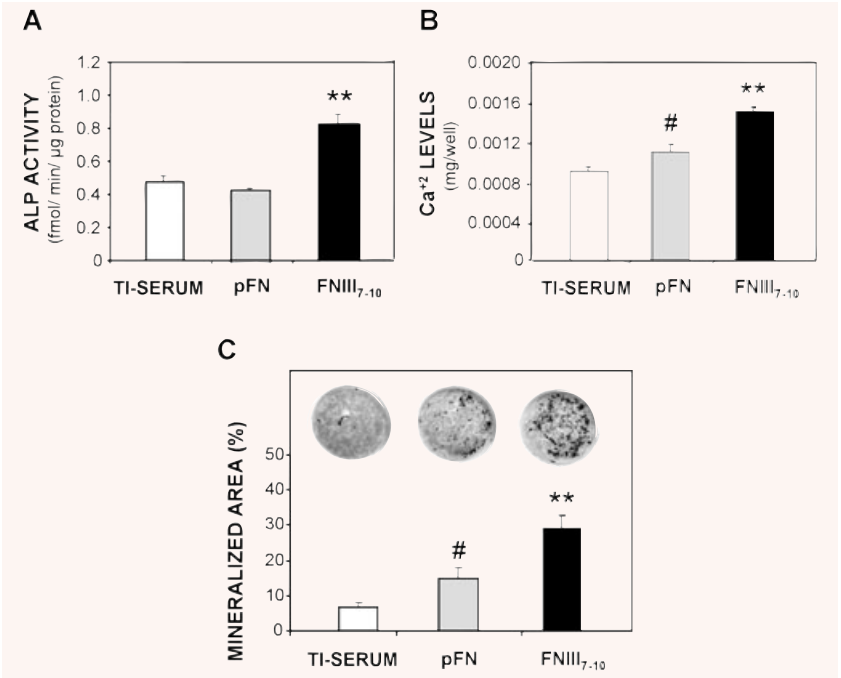

Fig. 5 Bone marrow stromal cells on $FNIII_{7–10}$-treated surfaces exhibit higher levels of markers for osteoblastic differentiation after 7 days in culture and more advanced matrix mineralization than pFN-treated or serum-treated Ti (14d). (**A**) $FNIII_{7–10}$-treated surfaces enhance alkaline phosphatase activity ($N = 4$) at 7 days over pFN-treated or serum-treated Ti ($FNIII_{7–10}$: $^{**}P < 0.0001$ *versus* pFN, $^{**}P < 0.0001$ *versus* Ti-serum), (**B**) Calcium content was increased at 14 days ($N = 4$) on $FNIII_{7–10}$-treated surfaces over pFN or serum-treated Ti ($FNIII_{7–10}$: $^{**}P < 0.008$ *versus* pFN, $^{**}P < 0.0001$ *versus* Ti-serum). In addition, cells on pFN-treated surfaces also exhibited a significant increase in Ca^{+2} content over unmodified, serum-treated Ti ($^{\#}P < 0.04$), (**C**) Quantification (percentage mineralized area) of von Kossa staining for mineral nodule formation (black) on ligand-treated surfaces at 14 days. ($FNIII_{7–10}$: $^{**}P < 0.04$ *versus* pFN, $^{**}P < 0.005$ *versus* Ti-serum; pFN: $^{\#}P < 0.03$ *versus* Ti-serum).

surface condition) to determine the level of bone-implant apposition demonstrated >50% enhancement in bone apposition on $FNIII_{7–10}$-treated implants compared to unmodified Ti ($P < 0.01$) and over 25% compared to the pFN-treated Ti implants ($P < 0.03$) (Fig. 6D). In addition, pFN-coated implants exhibited increased bone apposition over unmodified Ti ($P < 0.05$).

The overall quality and degree of osseointegration can be most directly assessed by measuring the mechanical strength of implant–bone interaction. Accordingly, functional mechanical testing may be a vital functional predictor of long-term implant success and lifetime [56]. Pull-out mechanical testing ($N = 7–9$ implants per surface condition) revealed significantly higher mechanical fixation of the $FNIII_{7–10}$-treated implants over both pFN-treated (85%, $P < 0.05$) and unmodified Ti (290%, $P < 0.001$), the current clinical standard (Fig. 6E). Notably, implants coated with pFN also displayed higher fixation than the unmodified

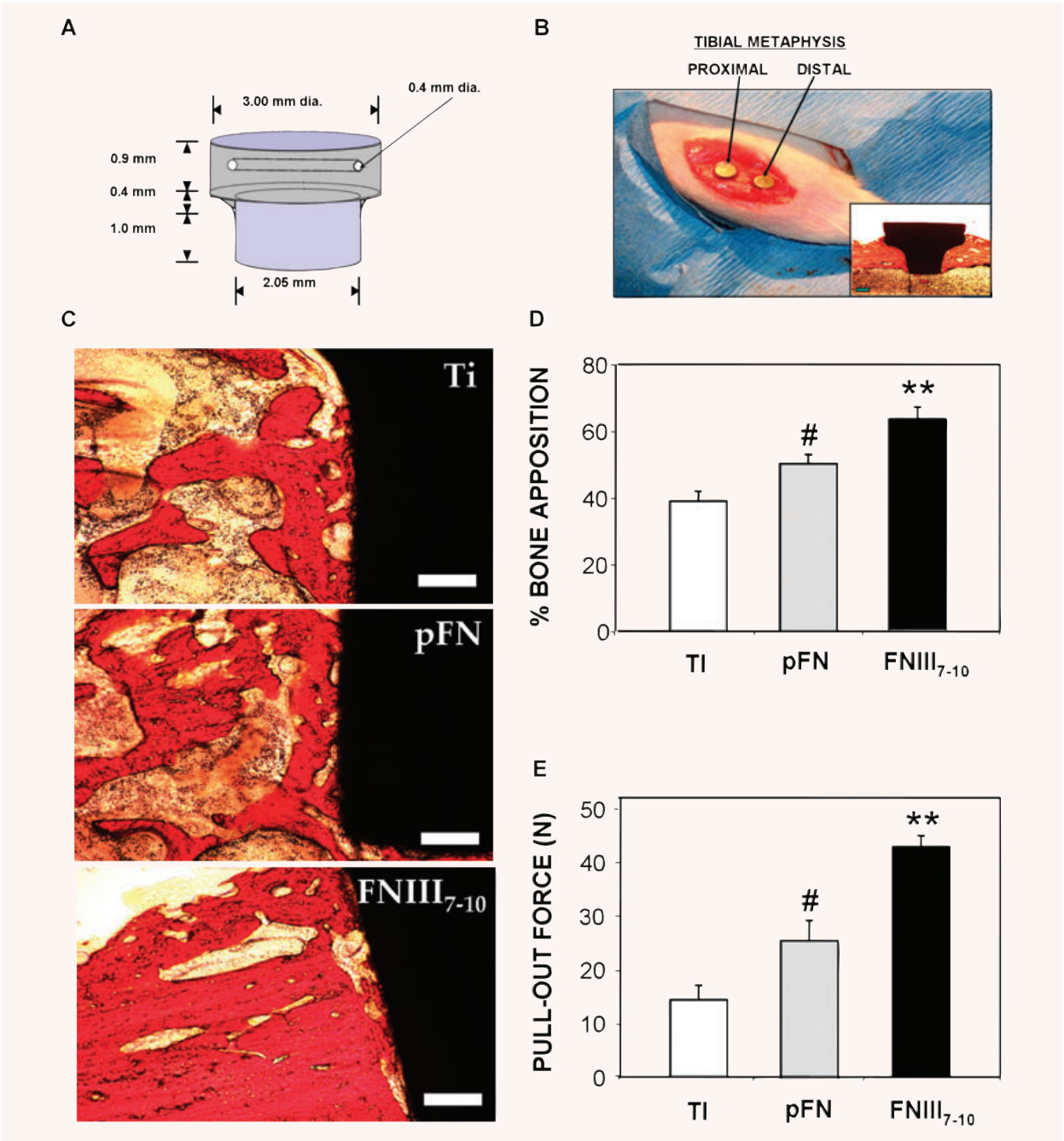

Fig. 6 Biomimetic ligand coatings targeting specific integrin receptors modulate *in vivo* implant osseointegration. (**A**) Schematic of titanium (clinical grade) implant design and dimensions. (**B**) Image of implants press fit into rat tibial metaphysis. Inset is a histological image of a slice of full implant and surrounding tissue (28 d after implantation). (**C**) Representative histological sections at 4 weeks after implantation showing bone (orange)-implant (black) contact (scale bar 0.2 mm). FNIII7–10-treated implant surfaces exhibited more contiguous bone tissue formation and connectivity compared to other surface treatment conditions. (**D**) Quantification of bone-implant contact area. Bone apposition was quantified from histological sections as the percentage of the implant's circumference in direct contact with bone tissue. For each implant, eight fields were quantified, and multiple slices of the same implant were averaged ($N = 4$ implants per surface condition) ($FNIII_{7–10}$: $^{**}P < 0.03$ *versus* pFN, $^{**}P < 0.01$ *versus* Ti-serum; pFN: $^{\#}P < 0.05$ *versus* Ti-serum). (**E**) Functional osseointegration as determined by pull-out force. There were seven to nine different implants for each surface condition ($FNIII_{7–10}$: $^{**}P < 0.05$ *versus* pFN, $^{**}P < 0.0001$ *versus* Ti-serum; pFN: $^{\#}P < 0.04$ *versus* Ti-serum.

Ti implants (66%, $P < 0.04$), although to a much lower extent than $FNIII_{7–10}$-coated implants. Collectively, these data corroborate *in vitro* results and demonstrate that a simple-to-apply bioactive coating using this $\alpha_5\beta_1$ integrin-specific ligand $FNIII_{7–10}$ can significantly enhance implant integration into the host bone to a greater degree over coatings of incorporating native full-length pFN and even more potently over the current clinical standard (unmodified Ti).

Discussion

This study examined the ability of a clinically translatable and simple biomolecular implant coating strategy to promote bone tissue healing and implant osseointegration. These coatings rely on the physisorption of FN-based ligands onto biomedical-grade Ti substrates. Given the functional importance of integrin receptors in modulating a variety of osteogenic pathways *in vitro*, promising surface coating strategies have sought to specifically promote integrin-mediated adhesion and signalling in a bone defect site [8]. These strategies often employ functionalizing implant surfaces with adhesive ligands consisting of matrix proteins (*e.g.* FN, collagen) or peptides derived from important bone matrix molecules (*e.g.* RGD motif from FN). However, these approaches have only marginally improved bone formation. Possible explanations for the corresponding lack of improvement in *in vivo* bone formation include non-specific responses to biological macromolecules with multiple bioactive motifs that may provide antagonistic signals (*e.g.* fibrinogen- and complement-binding activities in pFN) and insufficient pro-healing signalling due to lack of integrin specificity. Here, we demonstrate that an integrin-specific biomolecular surface strategy, using simple passive adsorption on Ti substrates of a fragment of FN that primarily engages integrin $\alpha_5\beta_1$, represents an effective approach for functional bone healing. This FN-mimetic orthopaedic implant coating confers integrin-specific cues to stem-like cells that enhance *in vitro* adhesion, proliferation and osteogenic signalling compared to the current clinical standard (unmodified Ti) as well as full-length FN-based coatings. These findings are consistent with results from an *in vitro* long-term differentiation study conducted with function-perturbing β_1 and β_3 antibodies on osteoblast-like cells [32]. Moreover, this biomimetic treatment also promoted elevated expression of osteoblast-specific genes, alkaline phosphatase activity and matrix mineralization and calcification, indicative of a surface-dependent pro-osteoblastic differentiation effect. Finally, as a clinical validation of this surface strategy, cortical bone implantation studies revealed greater contiguous bone contact area around $FNIII_{7–10}$-treated Ti implants compared to plasma FN and uncoated Ti implants. Most importantly, these *in vivo* studies also demonstrated significant improvements in mechanical fixation and functional osseointegration of this FN-mimetic surface coating over full-length pFN-treated Ti implants (twofold greater) and, notably, unmodified Ti implants (threefold greater). Notably, this $FNIII_{7–10}$-mediated enhancement of functional osseointegration may be potentially even greater because the $FNIII_{7–10}$ implant surface density was below the saturation level demonstrated by SPR.

We attribute the enhanced functional integration of the $\alpha_5\beta_1$-specific $FNIII_{7–10}$-implant coatings to increased cell recruitment and osteoblastic differentiation at the cell–material interface. Indeed, recent *in vivo* work suggests that ECM-coated implants may promote implant integration at early time points by modulating endogenous stromal cell chemotaxis to the implant surface very early (<3 days) after implantation [57]. Because endogenous bone cells can quickly remodel their underlying adherent surface [58], potentially masking these integrin-specific surface cues, these surface cues may act very early to differentiate cells in the bone remodelling process after implantation. In addition, surface-contacted cells may pass along osteogenic signals to more distant cell populations *via* cell–cell contact or secreted soluble biological factors, further influencing the tissue healing over a more extensive spatial and temporal range.

The differences in *in vitro* osteoblastic activities and *in vivo* bone formation between implants coated with $FNIII_{7–10}$ and pFN were unexpected because these two ligands present the 7th–10th type III repeats of FN. The recombinant $FNIII_{7–10}$ fragment, however, isolates the biological activity to this integrin binding site, whereas the full pFN molecule contains additional sites that may affect the osteoblastic differentiation and bone healing responses. In addition, our *in vitro* results with a receptor-mimetic antibody and integrin binding analyses suggest that the passively adsorbed recombinant fragment is more active than the full native protein (Fig. 1). This difference in biological activity could arise from difference in the structure/orientation of the adsorbed protein. Finally, it is worthwhile to note that the recombinant fragment lacks significant post-translational modifications (*e.g.* glycosylation) compared to the native protein which could influence its biological activity.

Importantly, this biomimetic surface approach utilizes a simple, point-of-care dip-coating of $FNIII_{7–10}$ to pre-sterilized Ti implants, a quick and versatile surface application conducted under physiological conditions that the surgeon can employ seconds before implantation. This single-step procedure, in turn, minimizes the chance of infection, reduces implant surface treatment variability, and minimizes cytotoxicity concerns inherent with covalent immobilization schemes, while maintaining the surgeon's dexterity. The more robust osseointegration demonstrated for $FNIII_{7–10}$-treated implants is expected to improve implant function and lifetime. Moreover, this straightforward coating protocol can be applied to virtually any dental and orthopaedic implant application. This $FNIII_{7–10}$ coating retains its bioactivity when dip-coated on a variety of other non-Ti material surfaces with different surface topographies, including other metals, polymers and ceramics. Furthermore, it may be advantageous to employ this biomimetic coating in conjunction with other implant surface technologies such as surface topography/roughness, calcium phosphate coatings, bone morphogenetic proteins and anti-inflammatory agents, in order to potentiate healing responses [59, 60].

In summary, $\alpha_5\beta_1$-specific $FNIII_{7-10}$ biomolecular coatings significantly enhance *in vitro* osteoblastic differentiation and implant osseointegration in a rat cortical bone model over full-length FN coatings and the clinical orthopaedic 'gold standard'. Importantly, this biomolecular coating relies on simple physisorption of bioactive ligands onto biomedical-grade Ti as a simple, clinically translatable, implant biofunctionalization strategy to enhance tissue-healing responses.

Acknowledgements

This work was funded by the NIH (R01 EB-004496), Arthritis Foundation and Georgia Tech/Emory NSF ERC on the Engineering of Living Tissues (EEC-9731643). T.A.P. acknowledges support from the Medtronic Foundation. The authors gratefully acknowledge Wasatch Histo Consultants for histology and M. Mathews for implant machining.

References

1. **Ducheyne P, Qiu Q**. Bioactive ceramics: the effect of surface reactivity on bone formation and bone cell function. *Biomaterials*. 1999; 20: 2287–03.
2. **Bauer TW, Schils J**. The pathology of total joint arthroplasty. I. Mechanisms of implant fixation. *Skeletal Radiol*. 1999; 28: 423–32.
3. **Ripamonti U, Richter PW, Nilen RW, *et al.*** The induction of bone formation by smart biphasic hydroxyapatite tricalcium phosphate biomimetic matrices in the non-human primate Papio ursinus. *J Cell Mol Med*. 2008; 12: 1029–48.
4. **Bauer TW, Schils J**. The pathology of total joint arthroplasty.II. Mechanisms of implant failure. *Skeletal Radiol*. 1999; 28: 483–97.
5. **Dillow AK, Ochsenhirt SE, McCarthy JB, *et al.*** Adhesion of alpha5beta1 receptors to biomimetic substrates constructed from peptide amphiphiles. *Biomaterials*. 2001; 22: 1493–05.
6. **Chung EH, Gilbert M, Virdi AS, *et al.*** Biomimetic artificial ECMs stimulate bone regeneration. *J Biomed Mater Res A*. 2006; 79: 815–26.
7. **Hubbell JA**. Materials as morphogenetic guides in tissue engineering. *Curr Opin Biotechnol*. 2003; 14: 551–8.
8. **Bernhardt R, Van Den DJ, Bierbaum S, *et al.*** Osteoconductive modifications of Ti-implants in a goat defect model: characterization of bone growth with SR muCT and histology. *Biomaterials*. 2005; 26: 3009–19.
9. **Becker D, Geissler U, Hempel U, *et al.*** Proliferation and differentiation of rat calvarial osteoblasts on type I collagen-coated titanium alloy. *J Biomed Mater Res*. 2002; 59: 516–27.
10. **De RA, Virdi AS, Kuroda S, *et al.*** Local application of rhTGF-beta2 enhances peri-implant bone volume and bone-implant contact in a rat model. *Bone*. 2005; 37: 55–62.
11. **Sumner DR, Turner TM, Urban RM, *et al.*** Additive enhancement of implant fixation following combined treatment with rhTGF-beta2 and rhBMP-2 in a canine model. *J Bone Joint Surg Am*. 2006; 88: 806–17.
12. **Ho JE, Chung EH, Wall S, *et al.*** Immobilized sonic hedgehog N-terminal signaling domain enhances differentiation of bone marrow-derived mesenchymal stem cells. *J Biomed Mater Res A*. 2007; 83: 1200–8.
13. **Muller P, Bulnheim U, Diener A, *et al.*** Calcium phosphate surfaces promote osteogenic differentiation of mesenchymal stem cells. *J Cell Mol Med*. 2008; 12: 281–91.
14. **Logeart-Avramoglou D, Anagnostou F, Bizios R, *et al.*** Engineering bone: challenges and obstacles. *J Cell Mol Med*. 2005; 9: 72–84.
15. **Kneser U, Schaefer DJ, Polykandriotis E, *et al.*** Tissue engineering of bone: the reconstructive surgeon's point of view. *J Cell Mol Med*. 2006; 10: 7–19.
16. **Ripamonti U**. Osteoinduction in porous hydroxyapatite implanted in heterotopic sites of different animal models. *Biomaterials*. 1996; 17: 31–5.
17. **Lutolf MP, Hubbell JA**. Synthetic biomaterials as instructive extracellular microenvironments for morphogenesis in tissue engineering. *Nat Biotechnol*. 2005; 23: 47–55.
18. **Langer R, Tirrell DA**. Designing materials for biology and medicine. *Nature*. 2004; 428: 487–92.
19. **Reyes CD, Petrie TA, Burns KL, *et al.*** Biomolecular surface coating to enhance orthopaedic tissue healing and integration. *Biomaterials*. 2007; 28: 3228–35.
20. **Adams JC, Watt FM**. Regulation of development and differentiation by the extracellular matrix. *Development*. 1993; 117: 1183–98.
21. **Damsky CH**. Extracellular matrix-integrin interactions in osteoblast function and tissue remodeling. *Bone*. 1999; 25: 95–6.
22. **Garcia AJ, Reyes CD**. Bio-adhesive surfaces to promote osteoblast differentiation and bone formation. *J Dent Res*. 2005; 84: 407–13.
23. **Hynes RO**. Integrins: versatility, modulation, and signaling in cell adhesion. *Cell*. 1992; 69: 11–25.
24. **Clark EA, Brugge JS**. Integrins and signal transduction pathways: the road taken. *Science*. 1995; 268: 233–9.
25. **Takeuchi Y, Suzawa M, Kikuchi T, *et al.*** Differentiation and transforming growth factor-beta receptor down-regulation by collagen-alpha2beta1 integrin interaction is mediated by focal adhesion kinase and its downstream signals in murine osteoblastic cells. *J Biol Chem*. 1997; 272: 29309–16.
26. **Mizuno M, Fujisawa R, Kuboki Y**. Type I collagen-induced osteoblastic differentiation of bone-marrow cells mediated by collagen-alpha2beta1 integrin interaction. *J Cell Physiol*. 2000; 184: 207–13.
27. **Moursi AM, Globus RK, Damsky CH**. Interactions between integrin receptors and fibronectin are required for calvarial osteoblast differentiation in vitro. *J Cell Sci*. 1997; 110: 2187–96.
28. **Luthen F, Lange R, Becker P, *et al.*** The influence of surface roughness of titanium on beta1- and beta3-integrin adhesion and the organization of fibronectin in human osteoblastic cells. *Biomaterials*. 2005; 26: 2423–40.
29. **Roche P, Goldberg HA, Delmas PD, *et al.*** Selective attachment of osteoprogenitors to laminin. *Bone*. 1999; 24: 329–36.
30. **Gronthos S, Simmons PJ, Graves SE, *et al.*** Integrin-mediated interactions between human bone marrow stromal precursor cells and the extracellular matrix. *Bone*. 2001; 28: 174–81.
31. **Cheng SL, Lai CF, Fausto A, *et al.*** Regulation of alphaVbeta3 and alphaVbeta5 integrins by dexamethasone in normal human osteoblastic cells. *J Cell Biochem*. 2000; 77: 265–76.
32. **Keselowsky BG, Collard DM, Garcia AJ**. Integrin binding specificity regulates biomaterial surface chemistry effects on cell

differentiation. *Proc Natl Acad Sci USA*. 2005; 102: 5953–7.
33. **Garcia AJ, Keselowsky BG**. Biomimetic surfaces for control of cell adhesion to facilitate bone formation. *Crit Rev Eukaryot Gene Expr*. 2002; 12: 151–62.
34. **Schneider GB, Zaharias R, Stanford C**. Osteoblast integrin adhesion and signaling regulate mineralization. *J Dent Res*. 2001; 80: 1540–4.
35. **Docheva D, Popov C, Mutschler W, *et al.*** Human mesenchymal stem cells in contact with their environment: surface characteristics and the integrin system. *J Cell Mol Med*. 2007; 11: 21–38.
36. **Guillot PV, Cui W, Fisk NM, *et al.*** Stem cell differentiation and expansion for clinical applications of tissue engineering. *J Cell Mol Med*. 2007; 11: 935–44.
37. **Liu YK, Uemura T, Nemoto A, *et al.*** Osteopontin involvement in integrin-mediated cell signaling and regulation of expression of alkaline phosphatase during early differentiation of UMR cells. *FEBS Lett*. 1997; 420: 112–6.
38. **Lynch MP, Stein JL, Stein GS, *et al.*** The influence of type I collagen on the development and maintenance of the osteoblast phenotype in primary and passaged rat calvarial osteoblasts: modification of expression of genes supporting cell growth, adhesion, and extracellular matrix mineralization. *Exp Cell Res*. 1995; 216: 35–45.
39. **Moursi AM, Damsky CH, Lull J, *et al.*** Fibronectin regulates calvarial osteoblast differentiation. *J Cell Sci*. 1996; 109: 1369–80.
40. **Ferris DM, Moodie GD, Dimond PM, *et al.*** RGD-coated titanium implants stimulate increased bone formation *in vivo*. *Biomaterials*. 1999; 20: 2323–31.
41. **Schliephake H, Scharnweber D, Dard M, *et al.*** Effect of RGD peptide coating of titanium implants on periimplant bone formation in the alveolar crest. An experimental pilot study in dogs. *Clin Oral Implants Res*. 2002; 13: 312–9.
42. **Healy KE, Rezania A, Stile RA**. Designing biomaterials to direct biological responses. *Ann N Y Acad Sci*. 1999; 875: 24–35.
43. **Elmengaard B, Bechtold JE, Soballe K**. In vivo effects of RGD-coated titanium implants inserted in two bone-gap models. *J Biomed Mater Res A*. 2005; 75: 249–55.
44. **Elmengaard B, Bechtold JE, Soballe K**. In vivo study of the effect of RGD treatment on bone ongrowth on press-fit titanium alloy implants. *Biomaterials*. 2005; 26: 3521–6.
45. **Barber TA, Ho JE, De Ranieri A, *et al.*** Peri-implant bone formation and implant integration strength of peptide-modified p(AAM-co-EG/AAC) interpenetrating polymer network-coated titanium implants. *J Biomed Mater Res A*. 2007; 80: 306–20.
46. **Petrie TA, Capadona JR, Reyes CD, *et al.*** Integrin specificity and enhanced cellular activities associated with surfaces presenting a recombinant fibronectin fragment compared to RGD supports. *Biomaterials*. 2006; 27: 5459–70.
47. **Krebsbach PH, Kuznetsov SA, Bianco P, *et al.*** Bone marrow stromal cells: characterization and clinical application. *Crit Rev Oral Biol Med*. 1999; 10: 165–81.
48. **Aubin JE**. Osteoprogenitor cell frequency in rat bone marrow stromal populations: role for heterotypic cell-cell interactions in osteoblast differentiation. *J Cell Biochem*. 1999; 72: 396–410.
49. **Reyes CD, Garcia AJ**. A centrifugation cell adhesion assay for high-throughput screening of biomaterial surfaces. *J Biomed Mater Res*. 2003; 67A: 328–33.
50. **Keselowsky BG, Garcia AJ**. Quantitative methods for analysis of integrin binding and focal adhesion formation on biomaterial surfaces. *Biomaterials*. 2005; 26: 413–8.
51. **Cutler SM, García AJ**. Engineering cell adhesive surfaces that direct integrin alpha5beta1 binding using a recombinant fragment of fibronectin. *Biomaterials*. 2003; 24: 1759–70.
52. **Keselowsky BG, Collard DM, García AJ**. Surface chemistry modulates fibronectin conformation and directs integrin binding and specificity to control cell adhesion. *J Biomed Mater Res*. 2003; 66A: 247–59.
53. **Garcia AJ**. Get a grip: integrins in cell-biomaterial interactions. *Biomaterials*. 2005; 26: 7525–9.
54. **Tamura Y, Takeuchi Y, Suzawa M, *et al.*** Focal adhesion kinase activity is required for bone morphogenetic protein–Smad1 signaling and osteoblastic differentiation in murine MC3T3-E1 cells. *J Bone Miner Res*. 2001; 16: 1772–9.
55. **Ducy P, Zhang R, Geoffroy V, *et al.*** Osf2/Cbfa1: a transcriptional activator of osteoblast differentiation. *Cell*. 1997; 89: 747–54.
56. **Kay JF**. Designing to counteract the effects of initial device instability: materials and engineering. *J Biomed Mater Res*. 1988; 22: 1127–36.
57. **Jimbo R, Sawase T, Shibata Y, *et al.*** Enhanced osseointegration by the chemotactic activity of plasma fibronectin for cellular fibronectin positive cells. *Biomaterials*. 2007; 28: 3469–77.
58. **Aubin JE, Liu F**. The osteoblast lineage. In: Bilezikien JP, Raisz LG, Rodan GA, editors. Principles of bone biology. San Diego: Academic Press; 1996. pp. 69–88.
59. **Ripamonti U, Richter PW, Thomas ME**. Self-inducing shape memory geometric cues embedded within smart hydroxyapatite-based biomimetic matrices. *Plast Reconstr Surg*. 2007; 120: 1796–807.
60. **Ripamonti U**. Soluble osteogenic molecular signals and the induction of bone formation. *Biomaterials*. 2006; 27: 807–22.